RESEARCH ARTICLE | DECEMBER 21 2005

1ω, 2ω, and 3ω methods for measurements of thermal properties

Chris Dames; Gang Chen

Rev. Sci. Instrum. 76, 124902 (2005)
https://doi.org/10.1063/1.2130718

1ω, 2ω, and 3ω methods for measurements of thermal properties

Chris Dames and Gang Chen
Department of Mechanical Engineering, Massachusetts Institute of Technology, 77 Massachusetts Avenue, Cambridge, Massachusetts 02139-4309

(Received 10 September 2005; accepted 3 October 2005; published online 21 December 2005)

3ω methods are commonly used to measure the thermal conductivity of a substrate adjacent to a strip heater or the thermal conductivity and specific heat of a suspended wire. Here we consider the general case of a line heater that is also used to sense temperature. Analysis of all harmonics is presented in terms of generic thermal and electrical transfer functions and is readily adapted to other experimental configurations. We identify voltage signals at 2ω and 1ω that contain the same information about the thermal properties as the 3ω signal. The 2ω voltage requires a dc offset at the current source. The 1ω voltage requires a very stable current source, but eliminates the need for higher-harmonic detection, and is advantageous for studying the dynamics of systems with very fast thermal response times. The 1ω, 2ω, and 3ω methods compare favorably with experiments using a suspended platinum wire and a line heater on a Pyrex substrate. With a modern lock-in amplifier, no common-mode voltage subtraction is necessary, which simplifies the experiment compared to the common practice of balancing a bridge or using a multiplying digital-to-analog converter. We also show that the widespread practice of using a voltage source to approximate a current source is only valid when the sample resistance is small compared to the total electrical resistance of the circuit, and derive and experimentally verify a correction factor to be used otherwise. © *2005 American Institute of Physics.* [DOI: 10.1063/1.2130718]

I. INTRODUCTION

3ω methods have proven to be valuable for measuring the thermal properties of various systems. In the basic method, a line heater is driven by a sinusoidal current source at angular frequency ω, causing a temperature fluctuation at 2ω related to the thermal properties of the heater and/or its surrounding environment. This perturbs the heater resistance at 2ω, leading to a voltage signal at 3ω. By varying the configuration of heater and its surroundings, 3ω methods have been used to measure the specific heat c (Refs. 1 and 2) and thermal conductivity k of a suspended wire,[3] k of solids[4] and thin films,[5,6] and k and c of liquids.[7,8] To achieve a good signal-to-noise ratio, the much larger Ohmic signal at 1ω is typically canceled either by nulling a bridge[1,2,8] or by subtraction with a multiplying digital-to-analog converter.[4] However, when using a lock-in amplifier with sufficient dynamic reserve, it is simpler to omit this cancellation step.[3] Another issue in implementing 3ω methods is that some lock-in amplifiers do not have third-harmonic detection built-in, requiring an external frequency tripler.[2,4,8]

A different class of experiments involves Joule heating a serpentine wire on a platform using a large direct current and measuring the resulting temperature rise using lock-in detection of a small alternating current superposed through the same heater. As reported by Shi *et al.*,[9] the proportionality between temperature and voltage can vary by a factor of 3 depending on the period of the ac sensing current compared to the thermal time constant of the system.

Here we unite the various traditional 3ω methods as well as the dc-heating/ac-detection experiments under a more general framework of thermal and electrical transfer functions. This framework can be applied to any thermal system containing a line heater that is also used to sense temperature. A related transfer function approach is used in hot-wire anemometry, with a focus on direct currents only.[10] Here, voltages at 1ω and 2ω are shown to contain the same information about thermal properties as the 3ω voltage does. The 2ω signal requires a dc offset at the driving current source. The 1ω signal eliminates the need for higher-harmonic detection and may also be useful for systems with very fast thermal response, such as nanowires. The 1ω, 2ω, and 3ω methods are verified experimentally using both a line heater on a Pyrex substrate and a suspended platinum wire, without any common-mode subtraction.

The usual 3ω analysis assumes that the circuit is driven with an ideal current source, but it is more common and convenient to use a voltage source instead. The important distinctions between current and voltage sources have not been adequately discussed in the literature. Here we also derive and verify a correction factor that permits the usual current-source analysis to be adapted to experiments performed with a voltage source. This correction factor is important whenever the electrical resistance of the sample is a significant fraction of the total resistance of the circuit.

II. GENERAL TRANSFER FUNCTION FRAMEWORK

A. Thermal transfer functions

We are interested in systems containing a single heater that is also used to sense temperature through changes in its electrical resistance. Such systems may be described quite

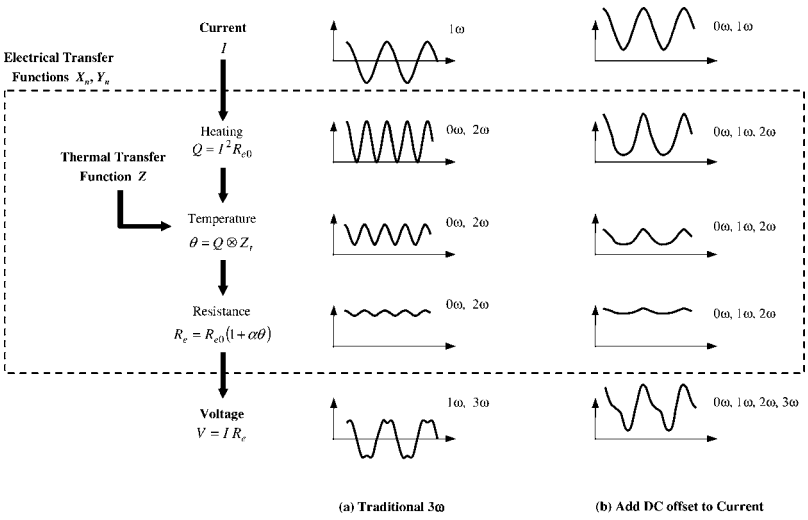

FIG. 1. Schematic relationship between current, voltage, and thermal transfer functions. (a) Traditional 3ω. (b) Addition of a dc offset to the driving current, resulting in additional terms for 1ω heating and 2ω voltage.

generally by a linear thermal transfer function Z, relating the average temperature rise of the heater θ_{avg} to the heat input Q. In the frequency domain,

$$\theta_\omega = Q_\omega Z, \tag{1}$$

where the ω subscript denotes Fourier-transformed quantities. In the time domain,

$$\theta_{\text{avg}}(t) = Q(t) \otimes Z_t, \tag{2}$$

where $\otimes$ denotes convolution and Z_t is the inverse Fourier transform of Z. For example, sinusoidal heating at frequency ω_H

$$Q(t) = Q_0 \sin(\omega_H t) \tag{3}$$

leads to a temperature response in the time domain

$$\theta_{\text{avg}}(t) = Q_0 \,\text{Re}[Z(\omega_H)]\sin(\omega_H t) + Q_0 \,\text{Im}[Z(\omega_H)]\cos(\omega_H t). \tag{4}$$

The thermal transfer function may be complex and frequency dependent. It contains information about the thermal properties of the system, such as thermal conductivity and/or specific heat of the heater and/or its surroundings.

B. Electrical transfer functions

By measuring the electrical current I and voltage V across the heater, we can determine the thermal properties of the system. First the thermal transfer function must be related to an electrical transfer function.

The traditional 3ω approaches are summarized in Fig. 1(a). A sinusoidal current at frequency ω leads to Joule heating with a 2ω component. The magnitude and phase of the resulting temperature rise at 2ω depend on Z. Due to the temperature coefficient of resistivity α, the electrical resistance of the heater also contains a modulation at 2ω. Finally, the current at ω mixes with the resistance at 2ω leading to a voltage signal at 3ω. Here we derive the analogous results for the more general case of a sinusoidal current with a dc offset. As shown in Fig. 1(b), we will see that the dc offset leads to additional Joule heating at 1ω and a voltage at 2ω.

In general, the electrical resistance of the heater is given by

$$R_e(t) = R_{e0}[1 + \alpha\theta_{\text{avg}}(t)], \tag{5}$$

where R_{e0} is the electrical resistance in the limit of zero current and θ_{avg} is averaged over the length of the heater. The temperature fluctuations within the heater must be small enough so that α may be treated as a constant. It is easily shown that Eq. (5) holds even if the temperature profile $\theta(x)$ varies along the length of the heater, as long as the cross section is uniform. Because $\alpha\theta_{\text{avg}} \ll 1$, to leading order Q can be approximated as

$$Q(t) = I^2(t)R_{e0}. \tag{6}$$

Combining Eqs. (5) and (6), the voltage drop across the heater is

$$V(t) = I(t)R_{e0}[1 + \alpha R_{e0} Z_t \otimes I^2(t)]. \tag{7}$$

Finally, using the frequency convolution theorem of Fourier transforms, the voltage in the frequency domain is given by

$$V_\omega = (R_{e0}/2\pi)I_\omega \otimes [2\pi\delta(\omega) + \alpha(R_{e0}/2\pi)(I_\omega \otimes I_\omega)Z], \tag{8}$$

where δ is the Dirac delta function.

Equation (8) applies to any current. Because it is nonlinear in I, we cannot use superposition and instead focus on the particular case of heating by a sinusoidal current at frequency ω_1 with a dc offset:

$$I(t) = I_{\text{dc}} + I_1 \sin(\omega_1 t), \tag{9}$$

where it is convenient to define

$$\eta = I_{\text{dc}}/I_1. \tag{10}$$

In the frequency domain,

$$I_\omega = I_1\{\eta 2\pi\delta(\omega) + j\pi[\delta(\omega+\omega_1) - \delta(\omega-\omega_1)]\}, \tag{11}$$

where $j = \sqrt{-1}$.

Applying this current to the analysis described above, the voltage response occurs at dc and three harmonics

$$V(t) = V_{\text{dc}} + V_{1\omega}(t) + V_{2\omega}(t) + V_{3\omega}(t), \tag{12}$$

which can be expressed as

TABLE I. $0\omega, 1\omega, 2\omega$, and 3ω electrical transfer functions defined by Eq. (14) for a thermal transfer function Z driven by current $I=I_1[\eta+\sin(\omega_1 t)]$. This very general result applies to any system with a line heater that is also used to measure temperature.

Harmonic n	In-phase electrical transfer function $[X_n(\omega_1,\eta)]$	Out-of-phase electrical transfer function $[Y_n(\omega_1,\eta)]$
0	0	$\eta\sqrt{2}\{\frac{1}{2\alpha R_{e0}I_{1,\mathrm{rms}}^2}+[\eta^2+(1/2)]Z(0)+\mathrm{Re}[Z(\omega_1)]\}$
1	$\frac{1}{2\alpha R_{e0}I_{1,\mathrm{rms}}^2}+[\eta^2+(1/2)]Z(0)+2\eta^2\,\mathrm{Re}[Z(\omega_1)]+(1/4)\mathrm{Re}[Z(2\omega_1)]$	$(1/4)\mathrm{Im}[Z(2\omega_1)]+2\eta^2\,\mathrm{Im}[Z(\omega_1)]$
2	$\eta(1/2)\{\mathrm{Im}[Z(2\omega_1)]+2\mathrm{Im}\,[Z(\omega_1)]\}$	$-\eta(1/2)\{\mathrm{Re}[Z(2\omega_1)]+2\mathrm{Re}[Z(\omega_1)]\}$
3	$-(1/4)\mathrm{Re}[Z(2\omega_1)]$	$-(1/4)\mathrm{Im}[Z(2\omega_1)]$

$$V(t)=\alpha R_{e0}^2 I_1^3\sum_{n=0}^{3}[X_n(\omega_1,\eta)\sin(n\omega_1 t)+Y_n(\omega_1,\eta)\cos(n\omega_1 t)], \tag{13}$$

where the summation is over the harmonics n. Here X_n and Y_n are the in-phase and out-of-phase electrical transfer functions. In terms of rms quantities as usually measured by lock-in amplifiers,

$$\frac{V_{n\omega,\mathrm{rms}}}{2\alpha R_{e0}^2 I_{1,\mathrm{rms}}^3}=X_n(\omega_1,\eta)+jY_n(\omega_1,\eta). \tag{14}$$

The resulting X_n and Y_n are given in Table I. This is the most important result of the article. It shows that the various electrical harmonics are rich with information about any thermal transfer function. For example, at 3ω the in-phase (X_3) and out-of-phase (Y_3) voltages are proportional to the real and imaginary parts of the thermal transfer function, respectively. Because they are a response to the Joule heating at twice the driving current, Z is probed at $2\omega_1$.

The 2ω voltages X_2 and Y_2 are only present in the case of a dc offset ($\eta\neq 0$). The in-phase 2ω voltage is sensitive to the imaginary part of Z, while the out-of-phase 2ω voltage is sensitive to the real part of Z. Furthermore, each 2ω voltage has contributions from the thermal response at both ω_1 and $2\omega_1$. This is because the Joule heating now has components at both $1\omega_1$ and $2\omega_1$, as seen in Fig. 1(b). The heating at $1\omega_1$ contributes a voltage at $2\omega_1$ after mixing with the $1\omega_1$ component of the current, and the heating at $2\omega_1$ also contributes a voltage at $2\omega_1$ after mixing with the dc component of the current.

The 1ω voltages X_1 and Y_1 are somewhat more complicated. Similar to Y_3, Y_1 has information about the imaginary part of $Z(2\omega_1)$, arising from the 2ω heating which is mixed back to 1ω by the 1ω component of the current. Whenever there is a dc offset in the current Y_1 has an additional contribution from $Z(\omega_1)$ due to the mixing of heating at 1ω and the direct current. The in-phase voltage X_1 has analogous contributions from both of these effects (the final two terms of X_1 in Table I) plus two other terms. The first term of X_1 is simply the large Ohmic response $V=I_1R_{e0}$, after normalizing according to Eq. (14). The second term of X_1, multiplying $Z(0)$, is the response to dc heating. This arises from both the dc offset (the η^2 term) and, importantly, the dc component of $[I_1\sin(\omega_1 t)]^2$.

The in-phase 1ω voltage is unique because it contains information about the dc thermal response even in the high-frequency limit. Because of thermal capacitance effects, most thermal transfer functions should become small at high frequencies. Thus X_2, X_3, Y_1, Y_2, and Y_3 should die out at high frequencies. But X_1 retains a term multiplying $Z(0)$, allowing the dc thermal response to be measured at high frequencies. This is because there is always a dc component in the I^2R heating, even at high frequencies. For example, with $I_{\mathrm{dc}}=0$ ($\eta=0$), the high-frequency limit of X_1 has an Ohmic voltage plus $Z(0)/2$, while in the low-frequency limit the contribution is $3Z(0)/4$. The opposite limit is $I_{\mathrm{dc}}\gg I_1$ ($\eta\gg 1$). In this case the high-frequency limit of X_1 is dominated by the contribution of $\eta^2 Z(0)$, while the dominant contribution at low frequency is $3\eta^2 Z(0)$. This shows that the factor of 3 difference between low- and high-frequency resistances reported by Shi *et al.*[9] ($\eta\sim 10$) is a general result, further indicating the broad applicability of the current transfer function framework.

Finally, in the presence of a dc offset in the current there is also a dc voltage across the sample. This is labeled as out of phase in Table I because of the convention introduced in Eq. (13). The three terms of Y_0 comprise a large Ohmic voltage, a contribution from the same dc heating as the second term of X_1, and the mixing of 1ω heating and 1ω current back to dc. These dc signals are not expected to be useful because they are subject to low-frequency drifts and thermoelectric voltages.

C. Current versus voltage source

The derivation above follows the usual assumption of an ideal current source at 1ω. In practice it often easier to use a voltage source, such as a function generator or the sine wave output of a lock-in amplifier. Although an operational amplifier circuit may be used to convert this voltage source to a current source,[3] it is more common to use the voltage source directly while analyzing the data as if a current source had been used. Here we show that this simplification is valid only if the sample resistance is small compared to the total resistance of the circuit and give a correction factor to use when the sample resistance is larger. Holland and Smith have also briefly considered the case of a voltage source for the special case of a suspended wire.[11]

Referring to Fig. 2(a), the total electrical resistance of the circuit R_{total} consists of the time-varying sample resistance $R_e(t)$ plus all other "ballast" resistances R_b, which are assumed constant over time. The ballast resistance includes the leads, the output impedance of the voltage source, and any additional resistors. For this voltage divider it is always true that

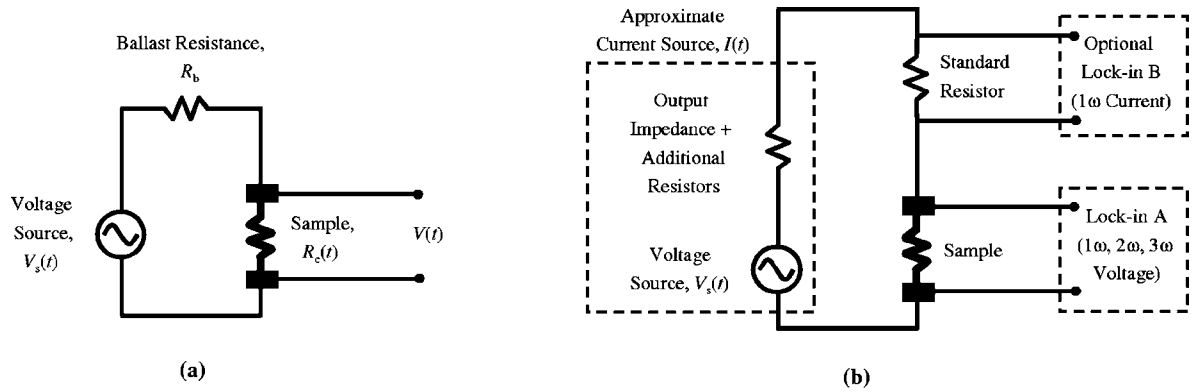

FIG. 2. (a) Circuit for analyzing the effects of using a voltage source rather than a current source which is usually assumed. (b) Schematic of equipment for simple $1\omega, 2\omega$, and 3ω experiments. No steps were taken to remove the large 1ω common-mode voltage. A voltage source was used to approximate a current source. Lock-in B was used to infer current from the voltage across a standard resistor. If lock-in B is omitted, the current can be estimated from the ratio of the source voltage to the total circuit resistance.

$$\frac{V(t)}{V_s(t)} = \frac{R_e(t)}{R_b + R_e(t)}, \tag{15}$$

where $V_s(t)$ is the time-varying voltage source.

In the usual way, we neglect the small resistance perturbations when calculating the Joule heating,

$$Q(t) \approx \frac{V^2(t)}{R_{e0}} = \frac{V_s^2(t)}{R_{e0}}\left(\frac{R_{e0}}{R_b + R_{e0}}\right)^2. \tag{16}$$

Equations (2) and (5) still hold, so

$$R_e(t) = R_{e0}[1 + \alpha Z_t \otimes Q(t)]. \tag{17}$$

The current through the circuit is then

$$I(t) = \frac{V_s(t)}{R_b + R_e(t)} \approx \frac{V_s(t)}{R_b + R_{e0}} \times \left[1 - \left(\frac{R_{e0}}{R_b + R_{e0}}\right)\alpha Z_t \otimes Q(t)\right], \tag{18}$$

where the negative sign arises from the leading-order Taylor-series expansion of $(1+\alpha Z_t \otimes Q)^{-1}$. This shows that, if R_{e0} is a small fraction of (R_b+R_{e0}), the true current is approximated well by the usually assumed $V_s/(R_b+R_{e0})$, but that an adjustment must be made otherwise. Comparing Eq. (18) with Eq. (7) further suggests that in the case of a voltage source at 1ω, it would be more appropriate to measure the harmonics of *current* to determine the thermal transfer function. Results analogous to Table I could be derived to give the electrical transfer function for a current in response to a voltage input of

$$V_s(t) = V_{s,\mathrm{dc}} + V_{s,1}\sin(\omega_1 t). \tag{19}$$

However, it is perhaps more useful to summarize this analysis by providing a correction factor to the results previously derived for a current source. To see this combine Eqs. (15) and (17), again using leading-order expansions, yielding

$$V(t) \approx V_s(t)\left(\frac{R_{e0}}{R_{e0} + R_b}\right)\left[1 + \left(\frac{R_b}{R_{e0} + R_b}\right)\alpha Q(t) \otimes Z_t\right]. \tag{20}$$

Finally, recognizing that the usual analysis assumes the current to be given by

$$I(t) \approx V_s(t)/(R_b + R_{e0}) \tag{21}$$

then the voltage across the sample can be expressed as

$$V(t) = I(t)R_{e0}\left[1 + \alpha R_{e0} I^2(t) \otimes Z_t\left(1 - \frac{R_{e0}}{R_{e0} + R_b}\right)\right]. \tag{22}$$

This is identical to Eq. (7), expect for the factor of $1 - R_{e0}/(R_{e0}+R_b)$ multiplying Z_t. Thus, even when using a voltage source, it is still possible to use the current-source analysis of Table I for data processing as long as the resulting calculated Z_{apparent} is corrected using

$$Z_{\mathrm{true}} = Z_{\mathrm{apparent}}\left(1 - \frac{R_{\mathrm{sample}}}{R_{\mathrm{total}}}\right)^{-1}. \tag{23}$$

The R_{sample} term should include all current-carrying resistances that exhibit 3ω harmonics, even if they lie outside the voltage probes, and thus may actually be larger than R_{e0}. This important point is clarified in Sec. IV C. The relative importance of the correction factor is seen to be the same as the relative contribution of the sample resistance to the total resistance of the circuit. This correction factor applies to any 3ω system using a voltage source for experiment but assuming a current source for data processing.

III. EXPERIMENT

To demonstrate the validity and generality of the analysis summarized in Table I and Eq. (23), these $1\omega, 2\omega$, and 3ω methods were applied to two traditional 3ω systems: an isolated suspended wire (SW) and a line heater on a substrate (LHOS). In the former system the goal is to measure both k and c of the heater itself, while in the latter system the goal is to measure k of the substrate.

The experimental apparatus is summarized in Fig. 2(b). The various voltage harmonics across the sample were measured using lock-in amplifier A (Stanford Research Systems SR850). A sinusoidal voltage source at 1ω was used to approximate a current source. The 1ω current was determined by measuring the 1ω voltage across a heat-sunk 10 Ω precision resistor (Vishay Dale, $\alpha \sim 10^{-5}$ K^{-1}) using lock-in B (SR830), which was also useful for precise phase corrections of the 1ω signals. The correction of Eq. (23) was applied

whenever the sample resistance was more than a few percent of the total circuit resistance. When dc offsets were required the voltage source was a function generator (HP 33120a); otherwise, the sine wave output of lock-in A was preferred to minimize phase errors.

Samples were mounted in a vacuum chamber and the temperature was controlled to 300 K (Lakeshore 330). Radiation losses were minimized by shielding, convection losses by operating in a vacuum of typically $\sim 10^{-5}$ torr, and conduction losses by using small diameter alloy wires for electrical connections. For the suspended-wire experiment the sample was a 50.8-μm (2 mil)-diam, 28.7-mm-long platinum wire (99.99% purity, $R_{e0} \sim 1.5\ \Omega$) soldered in a four-point configuration directly to the prongs of the sample holder. For the line-heater-on-substrate experiment, the sample was Pyrex, about 3 mm thick, with a microfabricated metal heater about 33 μm wide. The voltage drop was measured across the central 1000 μm ($R_{e0} \sim 54\ \Omega$) of the 3000-μm-long heater. For both systems the temperature coefficient of resistivity was determined by measuring the resistance at several temperatures between 300 and about 320 K.

Similar to the approach of Lu *et al.* for suspended wires[3] but counter to common practice for 3ω measurements, we have not used any noise cancellation scheme, such as nulling a bridge,[1,2,8] or subtraction of the voltage across a series resistor using a multiplying digital-to-analog converter.[4] This omission is successful only because of the high resolution and large dynamic reserve of lock-in A. With the optimal settings of maximum gain and minimum dynamic reserve, we routinely observe stable voltage steps of approximately 0.06 ppt of the full-scale sensitivity, corresponding to 1 part in 2^{14}. This is far better than the specified 1% absolute accuracy of the instrument and highlights an important detail when studying the 1ω signals: To avoid absolute errors between the various gain settings, we always keep the gain constant when sweeping frequency and/or amplitude at any one temperature point.

Other experimental details include dc coupling the input and turning off all line filters to keep from distorting these signals over the typical frequency range of 0.01–100 Hz. We assumed that the phase reported by lock-in B for the current represented the true value, and so some of the measurements were affected by phase disagreements between lock-ins A and B of $\sim 0.1°$. We have confirmed that the phase accuracy could be improved to $\sim 0.02°$ in the future by zeroing the phase of each lock-in at each frequency while driving a small-amplitude 1ω current. This is especially important for 1ω measurements and when using an external function generator. Finally, it is possible to omit lock-in B and instead measure the current simply by the ratio of the source voltage to the total resistance of the circuit. This gives a sufficient accuracy for most purposes, but requires knowledge of the circuit resistance at each temperature of measurement, and the resulting phase errors may degrade the out-of-phase 1ω signal.

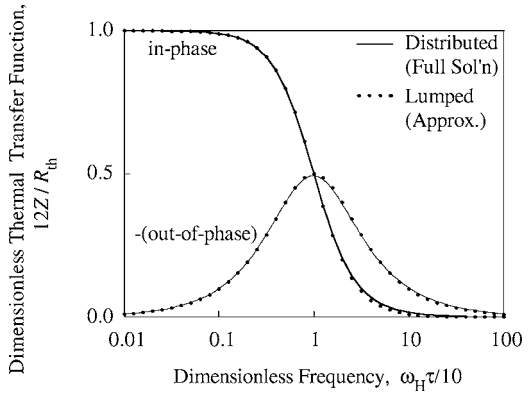

FIG. 3. Thermal transfer functions (average temperature rise per unit heat input) as a function of heating frequency for an isolated, suspended wire with thermally clamped ends. The transfer function is nondimensionalized using the thermal resistance $R_{th}=2l/kS$ and the frequency using the thermal diffusion time $\tau=4l^2/\kappa$. The solid lines are the exact solution, and the dots are a lumped approximation.

IV. RESULTS

The suspended-wire and line-heater-on-substrate systems are discussed separately. For each, the theoretical thermal and electrical transfer functions are first derived. Then, data are presented to validate the expected dependencies on alternating and direct currents. Finally, the measured electrical transfer functions are presented, and the corresponding thermophysical properties of platinum (k and c) and Pyrex (k) are extracted according to 1ω, 2ω, and 3ω methods independently. The correction factor of Eq. (23) is also verified below.

A. Suspended wire (SW)

1. Theoretical transfer functions

The thermal transfer function for an isolated SW with thermally clamped ends was given by Lu *et al.* as a series solution.[3] A closed-form solution for the spatial temperature profile is derived in Appendix A. The resulting thermal transfer function for a wire of length $2l$ and cross-sectional area S is

$$Z_{\mathrm{SW}}(\omega_H) = \frac{(\sinh\beta - \sin\beta) + j[\sinh\beta + \sin\beta - \beta(\cosh\beta + \cos\beta)]}{\beta C\omega_H(\cos\beta + \cosh\beta)}, \tag{24}$$

where C is the thermal capacitance of the wire,

$$\beta = \sqrt{\omega_H\tau/2}, \tag{25}$$

and characteristic diffusion time is

$$\tau = 4l^2/\kappa, \tag{26}$$

where κ is the thermal diffusivity.

This transfer function is depicted by the solid lines in Fig. 3. The shape is reminiscent of a lumped first-order (RC) system, so we are motivated to determine the lumped

TABLE II. Dimensionless $0\omega, 1\omega, 2\omega$, and 3ω electrical transfer functions defined by Eqs. (14) and (29) for the special case of a suspended wire in the lumped approximation [Eq. (31)].

Harmonic (n)	Dimensionless in-phase electrical transfer function $[\tilde{X}_{n,\mathrm{SW,lump}}(\tilde{\omega}_1, \eta)]$	Dimensionless out-of-phase electrical transfer function $[\tilde{Y}_{n,\mathrm{SW,lump}}(\tilde{\omega}_1, \eta)]$
0	0	$\eta\sqrt{2}\left[\frac{6}{\alpha R_{\mathrm{th}} R_{e0} I_{1,\mathrm{rms}}^2} + (\eta^2 + 1/2) + \frac{1}{1+\tilde{\omega}_1^2}\right]$
1	$\frac{6}{\alpha R_{\mathrm{th}} R_{e0} I_{1,\mathrm{rms}}^2} + (\eta^2 + 1/2) + \frac{(1/4)}{1+4\tilde{\omega}_1^2} + \eta^2 \frac{2}{1+\tilde{\omega}_1^2}$	$-\frac{(1/2)\tilde{\omega}_1}{1+4\tilde{\omega}_1^2} - \eta^2 \frac{2\tilde{\omega}_1}{1+\tilde{\omega}_1^2}$
2	$-(\eta/2)\left(\frac{2\tilde{\omega}_1}{1+4\tilde{\omega}_1^2} + \frac{2\tilde{\omega}_1}{1+\tilde{\omega}_1^2}\right)$	$-(\eta/2)\left(\frac{1}{1+4\tilde{\omega}_1^2} + \frac{2}{1+\tilde{\omega}_1^2}\right)$
3	$(-1/4)\frac{1}{1+4\tilde{\omega}_1^2}$	$(1/4)\frac{2\tilde{\omega}_1}{1+4\tilde{\omega}_1^2}$

transfer function $Z_{\mathrm{SW,lump}}$ that is the best approximation to Z_{SW}. As derived in Appendix B, the appropriate transfer function is

$$Z_{\mathrm{SW,lump}}(\omega_H) = \frac{R_{\mathrm{th}}}{12}\left[\frac{1 - j\omega_H\tau/10}{1 + (\omega_H\tau/10)^2}\right], \tag{27}$$

where the thermal resistance is

$$R_{\mathrm{th}} = 2l/kS. \tag{28}$$

As shown by the dots in Fig. 3, $Z_{\mathrm{SW,lump}}$ is an excellent approximation to Z_{SW} over most frequencies.

It is convenient to nondimensionalize Z_{SW}, X_n, and Y_n using $R_{\mathrm{th}}/12$:

$$\tilde{Z}_{\mathrm{SW}} = 12Z_{\mathrm{SW}}/R_{\mathrm{th}},$$

$$\tilde{X}_n = 12X_n/R_{\mathrm{th}},$$

$$\tilde{Y}_n = 12Y_n/R_{\mathrm{th}}. \tag{29}$$

Similarly, we define

$$\tilde{\omega}_H = \omega_H\tau/10. \tag{30}$$

Then Eq. (27) becomes

$$\tilde{Z}_{\mathrm{SW,lump}}(\tilde{\omega}_H) = \frac{1 - j\tilde{\omega}_H}{1 + \tilde{\omega}_H^2}. \tag{31}$$

The electrical transfer functions obtained by substituting Eq. (24) into Table I are easily evaluated but cumbersome to write out. On the other hand, Eq. (31) is so simple that it is worthwhile to give the electrical transfer functions explicitly for the lumped approximation (Table II). As shown in Fig. 4, the exact (solid lines) and lumped (dashed lines) electrical transfer functions are essentially identical at low frequencies and still agree very closely even at high frequencies. Although the data analysis in the present work uses the exact solution, the lumped solution is simpler to use and should be adequate for most purposes.

2. Current dependencies

The various electrical transfer functions of Table I show different scalings with I_1 and I_{dc} (through η). The scalings are compared with SW experiments in Fig. 5(a) for 3ω, Figs. 6(a) and 6(b) for 2ω, and Figs. 7(a)–7(d) for 1ω. Figure 5(a) confirms that at constant frequency, both in-phase (V_{X_3}) and out-of-phase voltages (V_{Y_3}) at 3ω are proportional to I_1^3. Similarly, Figs. 6(a) and 6(b) confirm that the 2ω voltages scale with I_1^3 and are linearly proportional to η.

Figures 7(a)–7(d) also show the expected scaling with I_1^3 and η^2. Figure 7(a), in particular, shows that the small change in V_{X_1} due to Joule heating can be distinguished from the much larger Ohmic signal, without any common-mode subtraction. The intercepts at $I_1=0$ of the two curves of Fig. 7(a) should in principle be identical, and the slight disagreement of approximately 1 ppt is an indication of the uncertainties in phase and amplitude at the two different frequencies. The fact that the $\eta=0$ intercepts of Fig. 7(d) are positive rather than negative as predicted by Table II is due to the phase error between lock-in A and the function generator. The phase uncertainty between lock-in A and lock-in B was typically $\sim 0.1°$, corresponding to a coupling of about 2 ppt from V_{X_1} into V_{Y_1}. Figure 7(c) shows that V_{X_1} was typically 10 mV, corresponding to an uncertainty of ~ 20 μV coupled into V_{Y_1}. This value is consistent with the offset in Fig. 7(d). Particularly for the 1ω methods, this shows that it is not the absolute values of X_n and Y_n, but rather their slopes with respect to I_1 and/or I_{dc}, that are most reliable for determining the thermal transfer functions.

3. Measured transfer functions

Having confirmed the expected dependencies on I_1 and I_{dc} at constant frequency, the electrical transfer functions at $1\omega, 2\omega$, and 3ω were then measured at constant current while sweeping the frequency. The results are compared to the theoretical transfer functions in Fig. 4. The lowest frequency measured was 0.01 Hz. Because of the long thermal diffusion time ($\tau \sim 30$ s), it was inconvenient to measure the data at lower $\omega\tau$ because of the long settling times involved.

For each harmonic, a least-squares fit was used to determine the R_{th} and τ that give the best match between measured and theoretical transfer functions. The fit was applied to both in-phase and out-of-phase transfer functions of a given harmonic simultaneously, although either could also be fitted separately. The thermal conductivity is calculated directly from R_{th} using Eq. (28). The specific heat is calculated from

$$c = \frac{\tau}{mR_{\mathrm{th}}}, \tag{32}$$

where m is the mass of the sample based on the measured geometry and the literature value of density. Because c involves two different experimentally measured parameters its uncertainty is larger than the uncertainty in k.

The resulting values of k and c are included in Fig. 4 and compared with literature values.[12] The values calculated

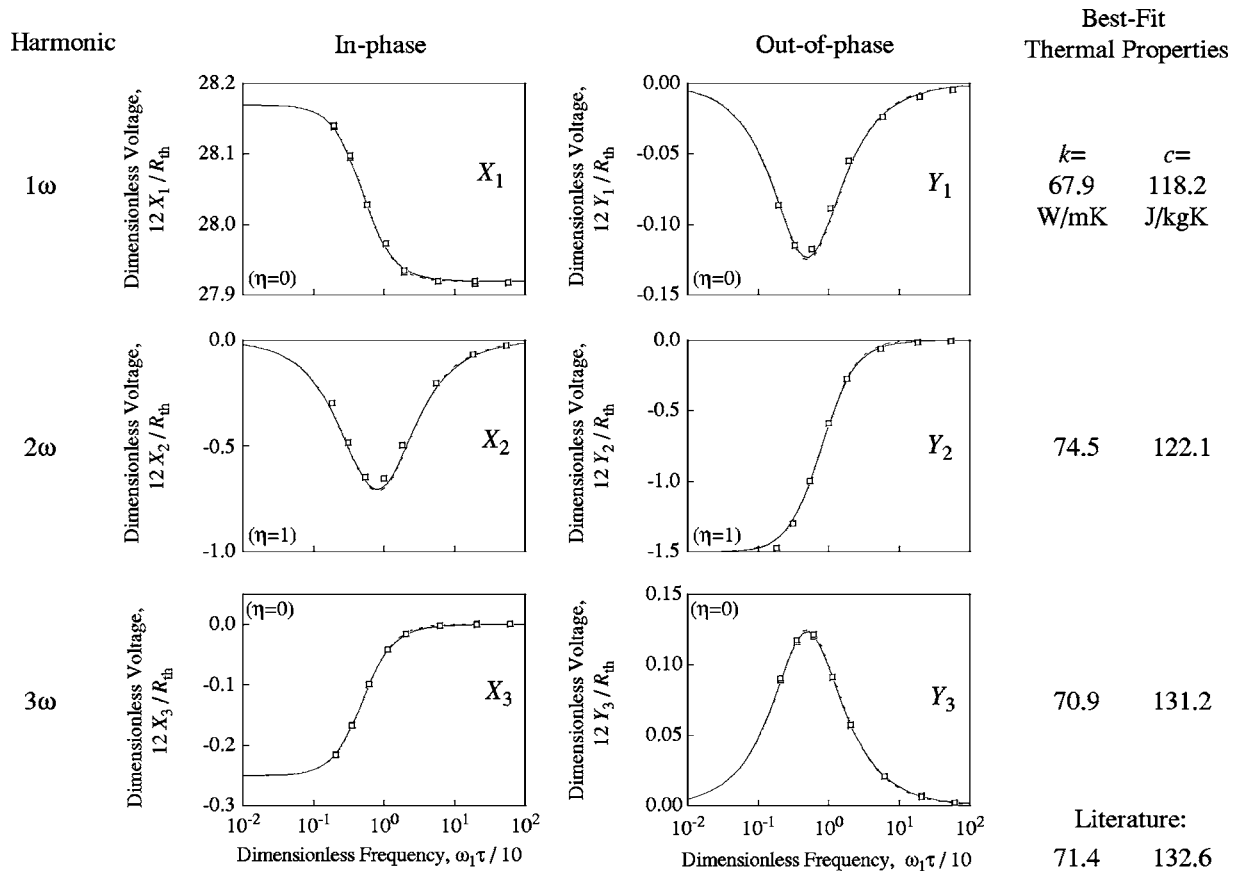

FIG. 4. 1ω, 2ω, and 3ω electrical transfer functions [voltage non-dimensionalized by Eq. (14)] for a suspended wire. The solid lines are the exact solution, the dashed lines are a lumped approximation, and the points are experimental data for a platinum wire at 300 K. The lumped approximation is almost indistinguishable from the exact solution. The values of thermal conductivity and specific heat used to fit the data from each harmonic are given on the right and compared with literature values (Ref. 12).

from the 3ω method are within about 1% of the literature values for both k and c. The errors in values calculated from 1ω and 2ω methods are somewhat worse, about 5% for k and 10% for c. This is consistent with the fact that there is slightly more scatter of the measured points about the theoretical curves of Fig. 4 for 1ω and 2ω. The increased uncertainty at 1ω may be due to the greater demands it places on the stability of both amplitude and phase of the voltage source (in this case lock-in A). The increased uncertainty at 2ω may be due to the necessity of using the external function generator as the voltage source.

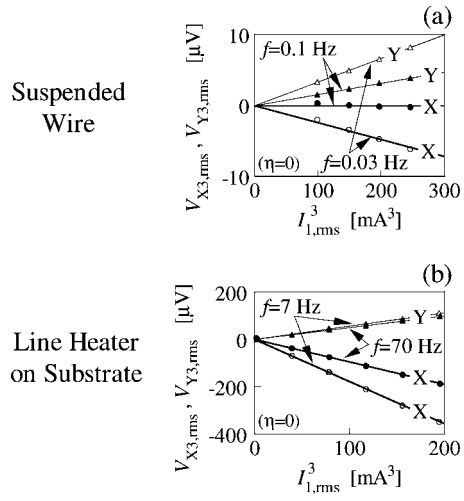

FIG. 5. 3ω voltage vs 1ω current, at constant frequency, showing the expected I^3 trend. (a) Suspended platinum wire at 300 K. (b) Line heater on a Pyrex substrate at 300 K.

B. Line heater on substrate (LHOS)

1. Theoretical transfer functions

The most widely known 3ω method is that popularized by Cahill,[4] Birge,[7] and Birge and Nagel[8] to measure the thermal conductivity of a substrate adjacent to a line heater. For the case of a heater of length L on a semi-infinite substrate of thermal conductivity k_{subs}, the thermal transfer function is given by[4]

$$Z_{\text{LHOS}}(\omega_H) = (-1/2\pi k_{\text{subs}} L)[\ln \omega_H + j\pi/2 + \text{const}], \quad (33)$$

where the unknown constant const is purely real, and the frequency must be such that the thermal wavelength $\lambda = (\kappa_{\text{subs}}/\omega_H)^{1/2}$ is large compared to the heater width yet small compared to the substrate dimensions. This transfer function is depicted in Fig. 8. When $\omega_H = 0$ Eq. (33) diverges, but $Z_{\text{LHOS}}(0)$ is actually limited to some finite value due to the finite substrate size. Table III gives the specific electrical transfer functions obtained by substituting Eq. (33) into Table I. They are depicted graphically by the solid lines in Fig. 9. For each harmonic, one of the (X_n, Y_n) signals is

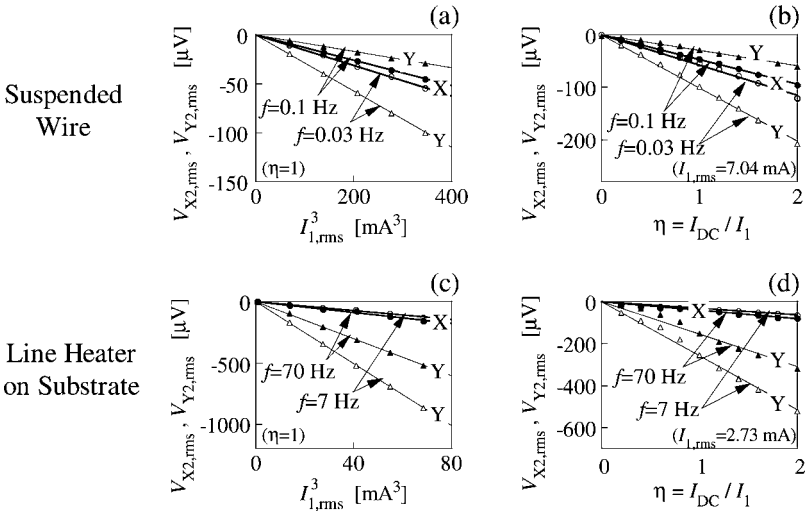

FIG. 6. (a) and (c) 2ω voltage vs 1ω current, at constant frequency and constant current ratio $\eta=I_{dc}/I_1$, showing the expected I^3 trend. (b) and (d) 2ω voltage vs current ratio $\eta=I_{dc}/I_1$, at constant frequency and constant I_1, showing the expected linear trend. (a) and (b) are for a suspended platinum wire at 300 K, while (c) and (d) are for a line heater on a Pyrex substrate at 300 K.

expected to vary linearly with ln ω_1, while the other signal is expected to be a constant.

2. Current dependencies

The scalings of the LHOS voltages with current at two different frequencies are shown in Fig. 5(b) for 3ω, Figs. 6(c) and 6(d) for 2ω, and Figs. 7(e)–7(h) for 1ω. Figure 5(b) shows that the 3ω voltages are proportional to I_1^3 as expected. Figure 6(c) shows that the 2ω voltages also scale with I_1^3 as expected. However, the scatter of the experimental points about the expected linear η dependence shown in Fig. 6(d) is larger than expected.

Figure 7(e) also shows the expected scaling with I_1^3, with the two resistance estimates (the intercepts at $I_1=0$) agreeing to better than 1 ppt. The out-of-phase voltages in Fig. 7(f) show a large scatter in discrete steps because they are at the limit of the sensitivity of the instrument. To detect the in-phase voltages [Fig. 7(e)] of ~300 mV the full-scale sensitivity was set to 500 mV. The 0.06 ppt voltage steps mentioned earlier are then 30 μV, consistent with the limiting resolution apparent in Fig. 7(f). The variation with I_{dc} in Figs. 7(g) and 7(h) shows the expected η^2 scaling for both in-phase and out-of-phase voltages. According to Table III, the two curves of Fig. 7(h) should be identical. The errors are due to the residual ~0.1° phase uncertainty between the function generator and lock-in A after using lock-in B for phase correction. This coupling of about 2 ppt of V_{X_1} into V_{Y_1} corresponds to about 400 μV of uncertainty in the intercept at $\eta=0$ in Fig. 7(h). Again, for the 1ω signals in particular, the slopes with respect to η^2 and/or I_1^3 are more reliable than the intercepts for determining thermal properties.

3. Measured transfer functions

Figure 9 compares the measured and theoretical electrical transfer functions at $1\omega, 2\omega$, and 3ω. For each harmonic the thermal conductivity was found by fitting the slope of the appropriate signal (X_1, Y_2, and X_3) with respect to ln ω_1. This is a generalization of the "slope method" commonly used in traditional 3ω analysis.[6] The other signal (Y_1, X_2, and Y_3) was not used in the fitting, and the measurements show large deviations from the theoretical value at $2\omega(-0.375)$ and especially at $1\omega(-0.0625)$. As with the suspended-wire system,

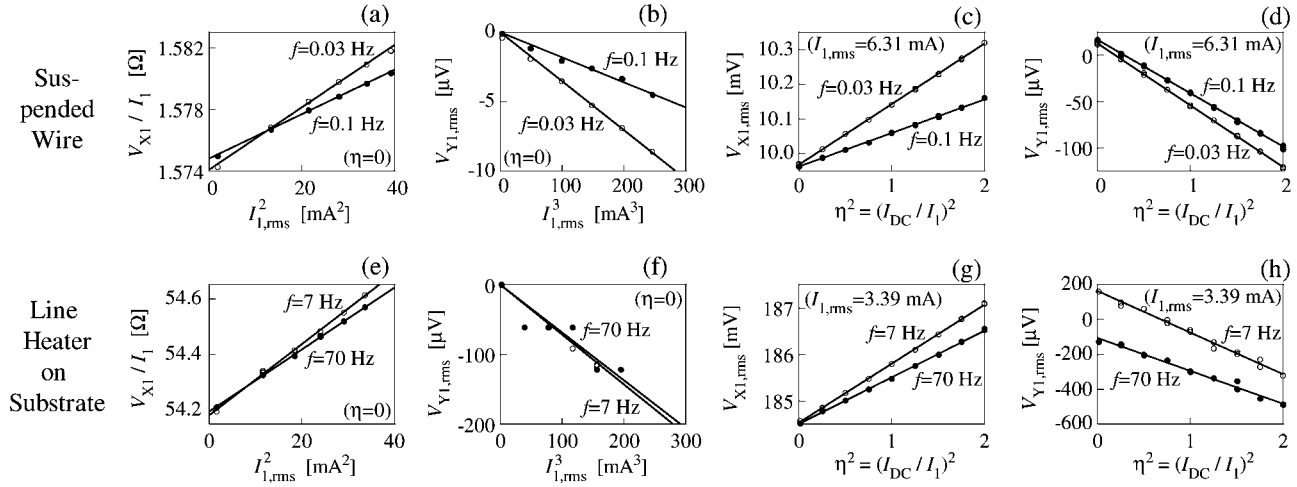

FIG. 7. (a) and (e) In-phase 1ω voltage vs 1ω current, at constant frequency, showing the expected trend of $a_1I_1+a_2I_1^3$. (b) and (f) Out-of-phase 1ω voltage vs 1ω current, at constant frequency, showing the expected I^3 trend. (c) and (g) In-phase 1ω voltage vs current ratio $\eta=I_{dc}/I_1$, at constant frequency and constant I_1, showing the expected trend of $a_3+a_4\eta^2$. (d) and (h) Out-of-phase 1ω voltage vs current ratio $\eta=I_{dc}/I_1$, at constant frequency and constant I_1, showing the expected trend of $a_5+a_6\eta^2$. (a)–(d) are for a suspended platinum wire at 300 K, while (e)–(g) are for a line heater on a Pyrex substrate at 300 K.

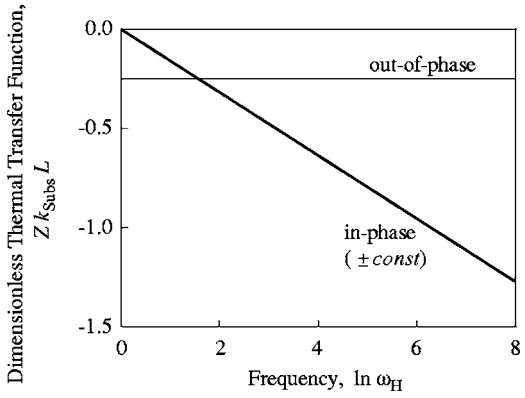

FIG. 8. Thermal transfer functions (average temperature rise per unit heat input) as a function of heating frequency for a line heater on a substrate. The transfer function is nondimensionalized using the product of the substrate's thermal conductivity k_{subs} and the heater length L. An arbitrary constant has been subtracted from the in-phase transfer function.

these deviations may be due to the phase disagreements between function generator and lock-in A at 2ω and the extreme sensitivity of Y_1 to phase errors. For the traditional 3ω method, Cahill also reported that the slope method gives more accurate results than using the magnitude of the constant out-of-phase voltage.[4]

The resulting values of thermal conductivity agree with each other to within 5% and are about 5%–10% higher than a literature value of 1.10 W/mK.[12] Again, the 1ω data show the largest scatter compared to the theoretical curve because of the large offset voltage which is not canceled. The root-mean-square deviation of the measurements in Fig. 9(a) from the theoretical curve is only about 0.02 ppt rms. However, this is enough to contribute significantly to the uncertainty because the total range of the data only spans approximately 0.5 ppt (439.73–439.95).

C. Current vs. voltage source

Figure 10 shows an example of measured thermal transfer functions both with and without the correction for using a voltage source instead of an ideal current source [Eq. (23)]. These data were taken by varying the additional resistors [Fig. 2(b)] in the line-heater-on-substrate experiment described above. Although only 3ω data are used in this example, the correction should be the same for any harmonic and any type of thermal transfer function that can be described using Table I. For each measurement, the total electrical resistance was determined along with the apparent thermal transfer function $Z_{apparent}$ calculated assuming an ideal current source according to Table III. Using the measured resistance ratio the thermal transfer function was corrected to $Z_{corrected}$ using Eq. (23). Finally, the average of these $Z_{corrected}$ was taken as the true thermal transfer function Z_{true}.

When making this correction it is essential to correctly account for the other portions of the electrical circuit which are subject to the same thermal transfer function as the test section. In this line-heater-on-substrate example, the voltage taps of the four-point probe at the sample only span the central 1000 μm of a 3000-μm-long heater line. However, the remaining 2000 μm of the heater still respond thermally in a similar way (neglecting end effects), so we may think of the effective sample as being 3000 μm long, with triple the resistance as measured by the four-point probe. In effect, those extra 2000 μm of current-carrying leads should not be counted as stable ballast resistance but instead exhibit a 3ω behavior like the sample resistance. Therefore, in this example, when making the correction of Eq. (23), $R_{sample}=3R_{e0}$. This can also be understood by considering the sample itself to be the 3000-μm-long line and simply multiplying the four-point probe voltages by a factor of 3. In the case of a suspended wire, however, this adjustment for leads should not be necessary, because any extra leads are likely to be heat sunk and/or have much lower resistance than the test section.

The raw and corrected Z of Fig. 10 are clearly in good agreement with the analysis of Eq. (23). The correction factor is unimportant when the sample resistance is negligible compared to the total resistance of the circuit. On the other hand, when the sample resistance is a significant fraction of the total resistance, the correction becomes large. The latter situation is undesirable because it is more sensitive to experimental uncertainties in measuring R_b and in measuring the unnecessarily small values of $X_{n,apparent}$, and $Y_{n,apparent}$. If a voltage source must be used with $R_{sample} \gg R_b$, it would be better to either measure the current harmonics directly as suggested in Eq. (18) or use an operational amplifier to implement a true current source.[3] In practice R_b is likely to be at least 50 Ω due to the output impedance of most voltage sources, suggesting that the correction of Eq. (23) may be an important consideration whenever R_{e0} is more than a few Ohms, unless additional ballast resistance is used.

Finally, we note that even with the widespread practice of common-mode subtraction it is still necessary to consider the correction for using a voltage source instead of a current source. This is evident from Eq. (22). To implement the common-mode subtraction a "series resistor" is introduced into the circuit.[4] This R_{series} is chosen to have nearly the same resistance as R_{e0}, but with good heat sinking and/or a small temperature coefficient so that its resistance is constant and voltage drop is always simply $I(t)R_{series}$. Lock-in A is then

TABLE III. $0\omega, 1\omega, 2\omega$, and 3ω electrical transfer functions defined by Eq. (14) for the special case of a line heater on a substrate [Eq. (33)]. The unknown constant const is the same for all terms.

Harmonic (n)	In-phase electrical transfer function $[X_{n,\mathrm{LHOS}}(\omega_1,\eta)]$	Out-of-phase electrical transfer function $[Y_{n,\mathrm{LHOS}}(\omega_1,\eta)]$
0	0	$\eta\sqrt{2}\left\{\frac{1}{2\alpha R_{e0} I_{\mathrm{I,rms}}^2}+[\eta^2+(1/2)]Z(0)-\frac{\ln\omega_1+\mathrm{const}}{2\pi k_{\mathrm{subs}}L}\right\}$
1	$\frac{1}{2\alpha R_{e0} I_{\mathrm{I,rms}}^2}+[\eta^2+(1/2)]Z(0)-(8\eta^2+1)\frac{\ln\omega_1+\mathrm{const}}{8\pi k_{\mathrm{subs}}L}-\frac{\ln 2}{8\pi k_{\mathrm{subs}}L}$	$(-1/16k_{\mathrm{subs}}L)(1+8\eta^2)$
2	$-3\eta/8k_{\mathrm{subs}}L$	$(\eta/4\pi k_{\mathrm{subs}}L)(3\ln\omega_1+\ln 2+3\ \mathrm{const})$
3	$(1/8\pi k_{\mathrm{subs}}L)(\ln\omega_1+\ln 2+\mathrm{const})$	$1/16k_{\mathrm{subs}}L$

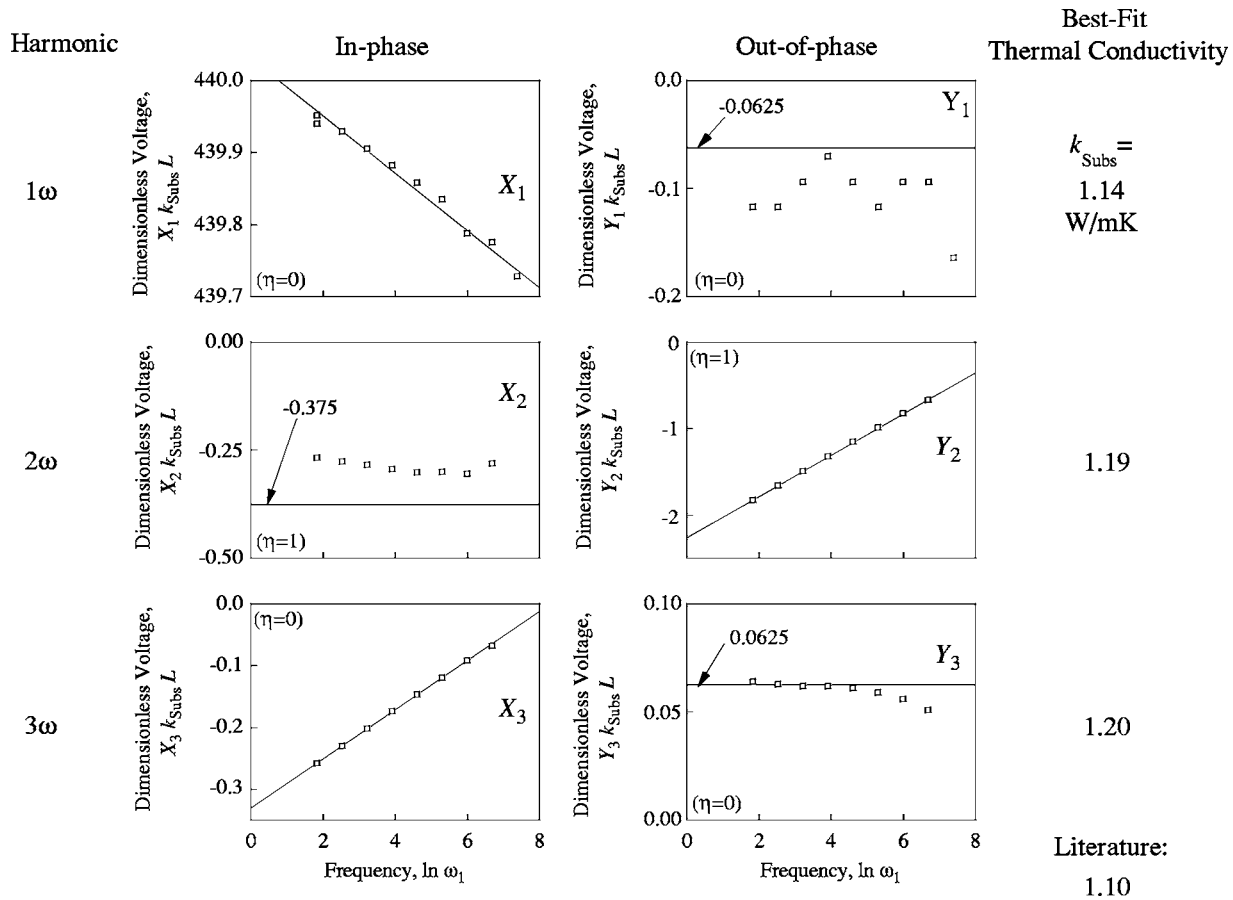

FIG. 9. $1\omega, 2\omega$, and 3ω electrical transfer functions [voltage non-dimensionalized by Eq. (14)] for a line heater on a substrate. The solid lines are the exact solution, and the points are experimental data for a Pyrex substrate at 300 K. The values of thermal conductivity used to fit the data from each harmonic are given on the right and compared to a literature value (Ref. 12).

used to measure the difference in voltage drops across the sample and the series resistor. This has the effect of canceling the first term in Eq. (22), but it does not affect the $[1 - R_{e0}/(R_{e0}+R_b)]$ term multiplying Z. Therefore the correction of Eq. (23) is still necessary.

V. DISCUSSION AND RECOMMENDATIONS

A. Selection of optimal dc offset

As shown in Table I, the voltage signals at 1ω and 2ω increase with increasing dc (increasing η). However, this also increases the common-mode voltage and the temperature variations within the sample, both of which may be undesirable. The optimum values of η for several different constraints are discussed below and summarized in Table IV.

1. Maximum signal for a limited temperature rise

The maximum temperature fluctuations of the sample θ_{max} should generally be limited to a few Kelvins in order to avoid ambiguity about the temperature of the measurement. This limits the currents as well. To simplify the analysis we assume that the experiment will include low frequencies, so that $Z(\omega)$ and $Z(2\omega)$ can be approximated with $Z(0)$. This should be the maximum value of Z. In this case the largest temperature rise is given by

$$\theta_{avg}(t) = [I_{dc} + I_1 \sin(\omega_1 t)]^2 R_{e0} Z(0) \tag{34}$$

leading to the constraint

$$I_1 + I_{dc} \leqslant I_{max}, \tag{35}$$

where $I_{max} = \sqrt{\theta_{max}/R_{e0}Z(0)}$.

From Table I and Eq. (14), the 3ω signals are not enhanced by I_{dc} and so should always operate with $\eta=0$. The 2ω voltages, on the other hand, are proportional to $I_1^2 I_{dc}$. Subject to Eq. (35), the optimum currents are found to be

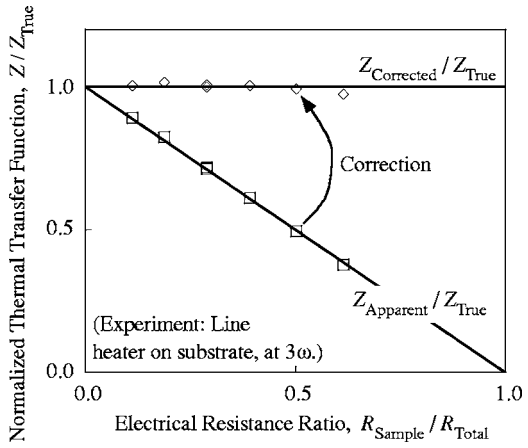

FIG. 10. Apparent and corrected thermal transfer functions (average temperature rise per unit heat input), according to Eq. (23). The sample resistance R_{sample} includes the full length of the line heater, which may be longer than the portion spanned by the voltage probes. This correction applies to any $1\omega, 2\omega$, or 3ω experiment that uses a voltage source but assumes a current source for analysis and data processing.

TABLE IV. Optimal values of the current ratio $\eta=I_{dc}/I_1$ for best signal, or signal-to-background ratio, for various harmonics. In some cases the optimum η depends on whether the dc portion of the voltage is filtered at the lock-in amplifier. The temperature rise is assumed to be constrained to $\theta_{avg}<\theta_{max}$, which is equivalent to constraining the total current $I_1+I_{dc}<I_{max}$. The experiment is further assumed to include low frequencies.

		At this harmonic			
To maximize	Filter dc at lock-in	1ω (in phase)	1ω (out of phase)	2ω	3ω
Signal	No filter	0	$1+\sqrt{5/8}=1.79\ldots$	1/2	0
Signal	Filter dc	0	$1+\sqrt{5/8}=1.79\ldots$	1/2	0
Signal-to-background ratio	No filter	0	$1+\sqrt{5/8}=1.79\ldots$	1/2	0
Signal-to-background ratio	Filter dc	∞	∞	1	0

$I_1=2I_{max}/3$ and $I_{dc}=I_{max}/3$, that is, $\eta=1/2$. With these optimizations, the 2ω and 3ω voltages have similar magnitudes for the two transfer functions considered in Tables II and III.

The useful part of the 1ω signals has terms proportional to $I_1I_{dc}^2$ as well as I_1^3. Optimization constrained by Eq. (35) now leads to $\eta=0$ to maximize the in-phase signal (V_{1X}) and $\eta=1+\sqrt{5/8}=1.791$ to maximize the out-of-phase signal (V_{1Y}). dc offsets are more important in the optimized V_{1Y} compared to the optimized V_{1X}, because the η^2 terms are relatively more important in Y_1 than in X_1.

2. Maximum signal-to-background for a limited temperature rise

Instead of maximizing the signal voltage itself, we may wish to maximize the signal-to-background ratio. This makes the best use of the gain and dynamic reserve of the lock-in amplifier, which is especially important when the common-mode subtraction is omitted, as in the present work. If the voltages are not filtered at the lock-in, then the peak background voltage for all harmonics is $I_{max}R_{e0}$, and the optimization for the maximum signal-to-background ratio is equivalent to the optimization for the maximum signal just discussed. However, if the dc component is filtered at the lock-in amplifier, then the background voltage contains only the Ohmic 1ω component I_1R_{e0}. In this case the 2ω signal-to-background ratio is optimized at $\eta=1$ and is approximately 1.5 times larger than the optimized 3ω signal-to-background ratio.

For the 1ω signal with dc filtering at the lock-in, the optimization leads to $\eta\rightarrow\infty$, i.e., a small ac sense current combined with a much larger dc-heating current.

3. Other limitations

Sometimes the experiment will be constrained by the current or voltage limits of the equipment. For example, the current will be limited when a voltage source is used with large ballast resistances to approximate a current source. In other cases the background signal voltages may be so large

TABLE V. Recommendations and comparison of 1ω, 2ω, and 3ω methods for thermal properties measurements.

	3ω ($I_{dc}=0$)	2ω ($I_{dc}\neq 0$)	1ω ($I_{dc}=0$)	1ω with dc offset ($I_{dc}\neq 0$)
Higher-harmonic detection	Requires third	Requires second	Not necessary	Not necessary
Current source	Use lock-in's own reference	Requires dc offset (extra hardware)	Use lock-in's own reference	Requires dc offset (extra hardware)
Stability of current source	Not important	Not important	Very important (subtracting two large numbers)	Very important (subtracting two large numbers)
Sensitivity to phase errors	Insensitive	Insensitive	Very sensitive	Very sensitive
Probes Z purely at one frequency or combines several	One frequency	Combines two	One frequency (plus dc)	Combines two (plus dc)
Frequency of voltage signal compared to heating	Higher (good for thermally slow systems)	Higher and same	Lower (good for thermally fast systems)	Lower and same
Precedents	Well established (Refs. 1–8)	New	New	$\eta\gg 1$ used previously (Ref. 9)
Recommendation	Most straightforward method. Use when not limited by fast system frequencies or need for third-harmonic detection.	Niche application: Use instead of 3ω when hardware has frequency doubler, but not frequency tripler, built-in.	Use for systems with very fast characteristic frequencies. Use to avoid implementing higher-harmonic detection. Be wary of phase errors.	Use for systems with very fast characteristic frequencies. Use to avoid implementing higher-harmonic detection. Be wary of phase errors.

as to saturate the input of the lock-in amplifier. These situations are equivalent to the $I_{\max}$ constraint already discussed. For a current-limited power supply, $I_{\max}$ is the equipment limitation, while for a voltage-limited power supply, $I_{\max}=V_{s,\max}/(R_{e0}+R_b)$. For a saturated lock-in, $I_{\max}=V_{\text{lock-in,max}}/R_{e0}$.

B. Relative merits of 1ω, 2ω, and 3ω methods

Some of the strengths and weaknesses of these 1ω, 2ω, and 3ω methods are outlined in Table V. The table highlights some important differences in the need for higher-harmonic detection, dc offset, and stability of the current source.

The various methods also have important distinctions when studying the frequency response of systems with very slow, or very fast, characteristic thermal times. For example, k and c of a single nanowire might be studied with the suspended-wire technique. However, the longitudinal thermal diffusion time is on the order of microseconds, corresponding to frequencies on the order of 100 s of kilohertz. To minimize the effects of parasitic inductances and capacitances, it is desirable to conduct the experiment at as low a frequency as possible. Table I shows that a 1ω study with $\eta=0$ probes the thermal response at twice the electrical detection frequency, in contrast to a 3ω study which probes the thermal response at 2/3 of the detection frequency. That is, the thermal response at 100 kHz is detected electrically at 50 kHz using 1ω, but at 150 kHz using 3ω. This shows that 1ω may be advantageous for systems with very fast dynamics. The argument is reversed for thermally very slow systems, where 3ω may be preferred.

Overall, the basic 3ω method is still the best option for most experiments. The 2ω method may be preferred for certain lock-in amplifiers which have frequency doubling built-in but not frequency tripling. 1ω methods place greater demands on the stability of the current supply, but eliminate the need for higher-harmonic detection, and are an important option when studying the dynamics of thermally fast systems. If a direct measurement of the thermal transfer function is desired, without combining the thermal response at multiple frequencies, then 3ω or 1ω with $\eta=0$ should be used.

VI. SUMMARY

We have developed a general transfer function framework (Table I) to describe any thermal system containing a line heater that is also used to sense temperature. This includes the traditional 3ω systems of a suspended wire (Fig. 4) and a line heater on a substrate (Fig. 9), as well as experiments combining a large dc-heating current with a small ac sense current.[9] The analysis naturally identifies 1ω, 2ω, and 3ω variations which each have their own benefits in certain situations (Table V).

Considering the excellent accuracy and dynamic reserve of modern lock-in amplifiers, it may no longer be necessary[3] to use noise cancellation via a bridge or multiplying digital-to-analog converter, making these experiments easier to implement [Fig. 2(b)].

Finally, the error introduced by using a voltage source to approximate a current source is shown to be equal to the ratio of the sample resistance to the total circuit resistance. A correction factor was derived [Eq. (23)] and verified (Fig. 10), allowing the usual current-source analyses to be adapted to the more common situation of a voltage-source experiment.

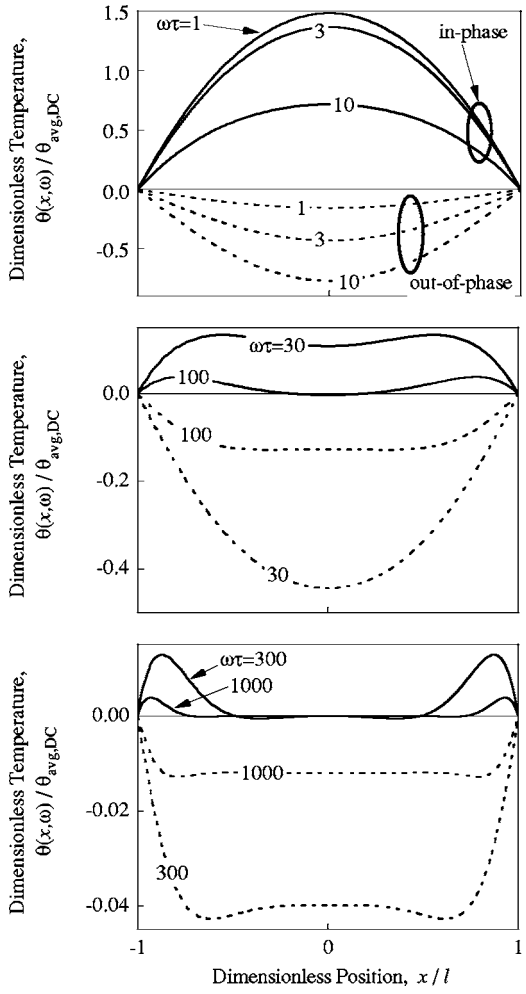

FIG. 11. Temperature profiles for a suspended wire driven by sinusoidal heating at various frequencies. The solid lines are the in-phase temperature, and the dashed lines are the out-of-phase temperature. The temperature rise is nondimensionalized by the average value at dc, and the frequency is nondimensionalized by the thermal diffusion time $\tau=4l^2/\kappa$. At low frequencies the response is large, parabolic, and in phase, while at high frequencies the response is smaller, flatter, and out of phase.

ACKNOWLEDGMENT

This work was supported by the NSF.

APPENDIX A: TEMPERATURE PROFILE IN A SUSPENDED WIRE

When a thin isolated wire is driven at a frequency much faster than the longitudinal thermal diffusion time the resulting temperature rise is related to c.[1,2,11] Similarly, the dc temperature rise is related to k.[13] A series solution for all frequencies was recently given by Lu *et al.*[3] Here we derive a closed-form solution and give a lumped approximation.

The unsteady, one-dimensional heat conduction equation neglecting convection and radiation losses, for a wire of length $2l$, is

$$\rho c \frac{\partial \theta}{\partial t} = k \frac{\partial^2 \theta}{\partial x^2} + \frac{Q(t)}{2Sl}. \tag{A1}$$

Here $\theta(x,t)$ is the temperature rise at a position x along the wire axis, and ρ is the density. The cross-sectional area of the wire is S, which must be constant but need not be circular. Assuming perfect thermal contact at $x=\pm l$, the boundary conditions are

$$\frac{\partial \theta(0,t)}{\partial x} = 0,$$

$$\theta(l,t) = 0. \tag{A2}$$

Taking the Fourier transform with respect to time and defining

$$W(x,\omega) = \theta_\omega - \frac{Q_\omega}{j\omega C}, \tag{A3}$$

the governing equation becomes

$$\frac{j\omega}{\kappa} W = \frac{\partial^2 W}{\partial x^2} \tag{A4}$$

with transformed boundary conditions

$$\frac{\partial W(0,\omega)}{\partial x} = 0, \quad W(l,\omega) = -\frac{Q_\omega}{j\omega C}. \tag{A5}$$

For heating given by Eq. (3), Eqs. (A3)–(A5) can be solved for θ. After considerable manipulation, the temperature profile in response to heating is found to be

$$\theta(x,t) = \left(\frac{Q_0}{C\omega_H}\right)\left\{\frac{-\sin[q_0(x+l)]\sinh[q_0(x-l)] - \sin[q_0(x-l)]\sinh[q_0(x+l)]}{\cos(2q_0 l) + \cosh(2q_0 l)}\right\}\sin(\omega_H t) + \left(\frac{Q_0}{C\omega_H}\right) \times \left\{\frac{\cos[q_0(x-l)]\cosh[q_0(x+l)] + \cos[q_0(x+l)]\cosh[q_0(x-l)]}{\cos(2q_0 l) + \cosh(2q_0 l)} - 1\right\}\cos(\omega_H t), \tag{A6}$$

where the thermal wave vector q_0 is given by

$$q_0 = \sqrt{\frac{\omega_H}{2\kappa}}. \tag{A7}$$

Temperature profiles are depicted in Fig. 11 for various frequencies. At low frequencies the temperature response is a quasistatic parabola typical of a uniformly heated wire in phase with the heating. At high frequencies the temperature profile is nearly flat and out of phase with the heating, because there is very little time for heat diffusion compared to the heating period. Interestingly, in the high-frequency case the peak value of temperature occurs not at the center but near the wire ends. This is also evident in the perturbation solution given by Holland and Smith for a semi-infinite wire.[11] It can be understood by considering the 90° phase difference between the heat source $Q(t)$ and conduction down the temperature gradient.

The spatially averaged temperature is given by

$$\theta_{\text{avg}}(t) = \left(\frac{Q_0}{C\omega_H}\right)\left\{\left[\frac{\sinh\beta - \sin\beta}{\beta(\cos\beta + \cosh\beta)}\right]\sin(\omega_H t) + \left[\frac{\sinh\beta + \sin\beta - \beta(\cosh\beta + \cos\beta)}{\beta(\cos\beta + \cosh\beta)}\right]\cos(\omega_H t)\right\}, \tag{A8}$$

where β is defined in Eq. (25). This leads directly to the transfer function given in Eq. (24).

APPENDIX B: LUMPED APPROXIMATION FOR SUSPENDED WIRE

Consider a lumped thermal mass with temperature $\theta_{\text{lump}}(t)$ and total heat capacity C_{lump} connected to $\theta_\infty = 0$ by an external thermal resistance $R_{\text{th,lump}}$. The well-known transfer function for this system is

$$Z_{\text{SW,lump}}(\omega_H) = R_{\text{th,lump}}\left[\frac{1 - j\omega_H \tau_{\text{lump}}}{1 + (\omega_H \tau_{\text{lump}})^2}\right]. \tag{B1}$$

As shown in Fig. 3, $Z_{\text{SW,lump}}$ is a remarkably good approximation to Z_{SW} over most frequencies as long as $R_{\text{th,lump}} = R_{\text{th}}/12$, and $\tau_{\text{lump}} = \tau/10$. These relations are justified mathematically by requiring $Z_{\text{SW,lump}}$ and Z_{SW} to have the same asymptotic behavior at low frequencies for both real and imaginary parts. These constraints are not unique. For example, if instead the correct magnitude of Z_{lump} was desired at both low and high frequencies, the constraints would be $R_{\text{th,lump}} = R_{\text{th}}/12$ and $\tau_{\text{lump}} = \tau/12$ (that is, $C_{\text{lump}} = C$).

An expression similar to Eq. (B1) was derived by Lu *et al.*[3] by retaining only the first term of a series expansion. In particular, Eqs. (14) and (B1) lead to

$$\sqrt{V_{X_3}^2 + V_{Y_3}^2} = \frac{\alpha R_{e0}^2 I_1^3 R_{\text{th}}}{24\sqrt{1 + (2\omega\tau/10)^2}}, \tag{B2}$$

which is slightly more accurate than Eq. (19) of Ref. 3. That equation has $\pi^4/4$ in place of 24 in the denominator (too large by 1.47%) and π^2 in place of 10 inside the radical (too small by 1.30%).

[1] L. A. Rosenthal, Rev. Sci. Instrum. **32**, 1033 (1961).
[2] L. R. Holland, J. Appl. Phys. **34**, 2350 (1963).
[3] L. Lu, W. Yi, and D. L. Zhang, Rev. Sci. Instrum. **72**, 2996 (2001).
[4] D. G. Cahill, Rev. Sci. Instrum. **61**, 802 (1990).
[5] D. G. Cahill, M. Katiyar, and J. R. Abelson, Phys. Rev. B **50**, 6077 (1994).
[6] T. Borca-Tasciuc, A. R. Kumar, and G. Chen, Rev. Sci. Instrum. **72**, 2139 (2001).
[7] N. O. Birge, Phys. Rev. B **34**, 1631 (1986).

[8] N. O. Birge and S. R. Nagel, Rev. Sci. Instrum. **58**, 1464 (1987).
[9] L. Shi, D. Li, C. Yu, W. Jang, D. Kim, Z. Yao, P. Kim, and A. Majumdar, J. Heat Transfer **125**, 881 (2003).
[10] A. E. Perry, *Hot-Wire Anemometry* (Oxford Science, Oxford, 1982).
[11] L. R. Holland and R. C. Smith, J. Appl. Phys. **37**, 4528 (1966).
[12] Thermophysical Properties Research Center, Purdue University, *Thermophysical Properties of Matter*, edited by Y. S. Touloukian (IFI/Plenum, New York, 1970).
[13] Y. C. Tai, C. H. Mastrangelo, and R. S. Muller, J. Appl. Phys. **63**, 1442 (1988).